1 **Localization, proteomics, and metabolite profiling reveal a putative vesicular**

2 **transporter for UDP-glucose**

3

4 Cheng Qian[1], Zhaofa Wu[2,3,6], Rongbo Sun[2,3,6], Huasheng Yu[2,3,4], Jianzhi Zeng[2,3,4], Yi

5 Rao[2,3,4,5], Yulong Li[2,3,4,5]*

6

7 [1]School of Life Sciences, Tsinghua University, 100084 Beijing, China

8 [2]State Key Laboratory of Membrane Biology, Peking University School of Life Sciences,

9 100871 Beijing, China

10 [3]PKU-IDG/McGovern Institute for Brain Research, 100871 Beijing, China

11 [4]Peking-Tsinghua Center for Life Sciences, 100871 Beijing, China

12 [5]Chinese Institute for Brain Research, Beijing 100871, China

13 [6]These authors contribute equally to this work

14 *e-mail: yulongli@pku.edu.cn

15

16 **Abstract**

17 Vesicular neurotransmitter transporters (VNTs) mediate the selective uptake and

18 enrichment of small molecule neurotransmitters into synaptic vesicles (SVs) and are

19 therefore a major determinant of the synaptic output of specific neurons. To identify

20 novel VNTs expressed on SVs (thus identifying new neurotransmitters and/or

21 neuromodulators), we conducted localization profiling of 361 solute carrier (SLC)

22 transporters tagging with a fluorescent protein in neurons, which revealed 40 possible

23 candidates through comparison with a known SV marker. We parallelly performed

24 proteomics analysis of immunoisolated SVs and identified 7 transporters in overlap.

25 Ultrastructural analysis confirmed one of the transporters, SLC35D3, localized to SVs.

26 Finally, by combining metabolite profiling with a radiolabeled substrate transport assay,

27 we identified UDP-glucose as the principal substrate for SLC35D3. These results

28 provide new insights into the functional role of SLC transporters in neurotransmission

29 and improve our understanding of the molecular diversity of chemical transmitters.

30

Introduction

The release of extracellular signaling molecules by secretory vesicles is a strategy used by a wide range of cell types and tissues and plays an essential role under both physiological and pathological conditions (Burgoyne and Morgan, 2003). A key step in the process is the accumulation of the respective signaling molecules into the secretory vesicles by specific transporter proteins. In the nervous system, vesicular neurotransmitter transporters (VNTs) such as VGLUT and VGAT (which transport glutamate and GABA, respectively) are essential for the transport of small molecule neurotransmitters into synaptic vesicles (SVs). These selective transporters determine the category, amount, and transport kinetics of neurotransmitters, thereby establishing the molecular basis of the underlying chemical neurotransmission (Blakely and Edwards, 2012). All VNTs identified to date belong to the Solute Carrier (SLC) superfamily of membrane transport proteins, the second-largest group of membrane proteins in the human proteome, with more than 400 members spanning 65 subfamilies (http://slc.bioparadigms.org/) (Hediger et al., 2013). Strikingly, approximately 30% of these 400 transporters are either uncharacterized or orphan transporters (Cesar-Razquin et al., 2015; Perland and Fredriksson, 2017), providing the opportunity to identify novel VNTs and their cognate substrates, thus identifying new neurotransmitters and/or neuromodulators.

The physiological role of transporter proteins is closely coupled to their subcellular localization; however, to date localization profiling of transporters—particularly SLC transporters, including which are expressed on secretory organelles in primary cells—

53 have not been systematically studied. Tagging a protein of interest with a fluorescent

54 protein is a widely used strategy for localization profiling (Chong et al., 2015; Huh et

55 al., 2003; Simpson et al., 2000), and this approach offers an effective strategy for

56 screening large numbers of targeted proteins. In addition, the development of mass

57 spectrometry (MS)–based proteomics coupled with subcellular fractionation has made

58 it possible to examine the subcellular spatial distribution of the proteome both rapidly

59 and efficiently (Andersen et al., 2003; Christoforou et al., 2016; Itzhak et al., 2016;

60 Orre et al., 2019), including the SV proteome (Laek et al., 2015; Takamori et al., 2006).

61 Immunoisolation of SVs, followed by proteomic analysis using high-sensitivity MS,

62 provides a specific and efficient method for characterizing the molecular anatomy of

63 SVs (Boyken et al., 2013; Gronborg et al., 2010) including endogenous SLC

64 transporters.

65   Electron microscopy (EM) is the gold standard to obtain ultrastructural information

66 since it offers the vastly superior resolution (on the order of 1 nm in biological samples)

67 compared to the resolution of optical imaging (on the order of 200-300 nm)

68 (Fernandez-Suarez and Ting, 2008). Moreover, using a genetically encoded tag for

69 EM overcomes certain limitations associated with classic immuno-EM labeling

70 methods, which require specific antibodies and penetration of those antibodies.

71 APEX2, an enhanced variant of ascorbate peroxidase, is a highly efficient proximity-

72 based EM tag (Lam et al., 2015) suitable for determining the subcellular localization

73 of proteins of interest.

74   Identifying the molecular function of an orphan transporter is an essential step

75   toward understanding its biological function. However, using the classic radiolabeled

76   substrate transport assay to deorphanize transporters is a relatively low-throughput

77   approach, particularly given the virtually unlimited number of chemicals that can be

78   tested. On the other hand, metabolite profiling using MS is a high-throughput method

79   for knowing the content metabolites (Chantranupong et al., 2020; Nguyen et al., 2014;

80   Vu et al., 2017) that can offer insights into candidate substrates. Thus, combining

81   metabolite profiling together with the radiolabeled substrate transport assay will likely

82   yield new insights into the molecular function of orphan transporters.

83   The nucleotide sugar uridine diphosphate glucose (UDP-glucose) plays an essential

84   role in glycosylation in both the endoplasmic reticulum and the Golgi apparatus

85   (Moremen et al., 2012). Interestingly, the release of UDP-glucose into the extracellular

86   space was detected previously using an enzyme-based method (Lazarowski et al.,

87   2003). Subsequent experiments with 1231N1 cells (an astrocytoma cell line) showed

88   that the release of UDP-glucose requires both Ca^{2+} signaling and the secretory

89   pathway, as the release was inhibited by the Ca^{2+} chelator BAPTA and the Golgi

90   apparatus blocker brefeldin A (Kreda et al., 2008).

91   Nucleotide sugars are transported into subcellular organelles by the SLC35 family,

92   which contains 31 members, including 20 orphan transporters (Caffaro and Hirschberg,

93   2006; Ishida and Kawakita, 2004; Song, 2013). Importantly, the level of nucleotide

94   sugars released by cells can be manipulated by changing the expression of SLC35

95   transporters; for example, knocking out an SLC35 homolog in yeast decreased the

96   release of UDP-*N*-acetyl-galactosamine, whereas overexpressing human SLC35D2 in

97   airway epithelial cells increased UDP-*N*-acetyl-galactosamine release (Sesma et al.,

98   2009). However, whether UDP-glucose is transported by a SLC35 transporter located

99   on secretory organelles is currently unknown.

100   In this study, we screened 361 SLC members using localization profiling and

101   identified 40 candidate vesicular transporters. In parallel, we performed proteomics

102   analyses of immunoisolated SVs from mouse brain samples and found that 7

103   transporters overlapped, including the orphan SLC35 subfamily transporters

104   SLC35D3, SLC35F1, and SLC35G2. Further ultrastructural analysis using APEX2-

105   based EM confirmed that the SLC35D3 traffics to SVs. Finally, we combined

106   metabolite analysis and the radiolabeled substrate transport assay in subcellular

107   organelles and identified UDP-glucose as the principal substrate of SLC35D3.

108

109   **Results**

110   ***Identification of a subset of SLC35 proteins as putative vesicular transporters***

111   ***using localization screening of SLC transporters***

112   To identify new candidate vesicular transporters, we performed localization screening

113   of SLC transporters (Figure 1). First, we created a cloning library containing 361

114   human SLC family members fused in-frame with the red fluorescent protein mCherry;

115   we then systematically co-expressed individual SLC-mCherry construct with EGFP-

116   tagged synaptophysin (SYP-EGFP) to label SVs in cultured rat cortical and

117   hippocampal neurons, revealing the localization of SLC transporters (Figure 1A,B). Of

118   the 223 SLC transporters that trafficked to neurites, 134 showed overlap with SYP-

119 EGFP and were analyzed further by quantifying the co-localization ratio between the

120 red and green fluorescent signals (Figure 1A,E). As expected, known synaptic

121 vesicular transporters such as VGLUT and the vesicular acetylcholine transporter

122 (VAChT) had relatively high co-localization ratio with SYP-EGFP (50-80% co-

123 localization) (Figure 1C,E), whereas markers of non-vesicular organelles such as the

124 Golgi apparatus, endoplasmic reticulum, and mitochondria had relatively low co-

125 localization ratio (10-20%) (Figure 1D,E). Setting a threshold at the colocalization ratio

126 for VGLUT3—a well-known vesicular transporter—revealed a total of 40 candidate

127 vesicular transporters (Figure 1E and Supplementary Table S1). Among these

128 candidates, a subset of SLC35 transporters, including SLC35D3, SLC35F1, and

129 SLC35G2, had a co-localization ratio of approximately 70% with SYP-EGFP (Figure

130 1E,F). In contrast, other members of the same subfamily such as SLC35A1, SLC35E1,

131 and SLC35E2, localized primarily to organelles in the soma and had relatively low co-

132 localization ratio (10%-20%) (Figure 1E,G). Together, these results indicate that

133 putative vesicular transporters, including a subset of SLC35 family members, localize

134 to neuronal SVs.

135

136 ***Proteomics analysis of SVs reveals novel vesicular transporters***

137 To probe the proteome including the vesicular transporters presented in SVs, we

138 immunoisolated intact SVs from fractionated mouse brain samples and used western

139 blot analysis and high-performance liquid chromatography (HPLC)-MS to analyze the

140 proteome (Figure 2A). Using a specific antibody against SYP to isolate SVs, we found

141   a number of SV markers present in the anti-SYP samples but not in samples obtained

142   using a control IgG (Figure 2B); as an additional control, the postsynaptic marker PSD-

143   95 was not detected in either the anti-SYP sample or the control IgG sample in western

144   blotting. Moreover, using EM we directly observed SVs on the surface of anti-SYP

145   beads but not control IgG beads (Figure 2C), confirming that the anti-SYP beads

146   selectively isolate SVs.

147   Next, we performed HPLC-MS analysis and found high reproducibility among

148   repeated trials in both the anti-SYP and control IgG samples (Supplementary Figure

149   S1). We further analyzed the relatively abundant proteins (LFQ intensity $>2^{20}$, without

150   immunoglobin) that were significantly enriched in the anti-SYP sample compared to

151   the control sample (Figure 2D). The proteins enriched in the anti-SYP sample covered

152   more than 60% of the 110 proteins in the SV proteome listed in the SynGO database

153   (Koopmans et al., 2019), including known VNTs, vesicular ATPase subunits, and a

154   number of other SV markers (Figure 2D-F). Conversely, only 8.0% and 2.2% of the

155   proteins in the mitochondrial and Golgi apparatus proteome, respectively, were

156   present in the anti-SYP sample (Figure 2F), indicating minimal contamination by these

157   organelles; as an additional control, we found very little overlap between the proteins

158   in the anti-SYP sample and the entire mouse proteome in the UniProt database

159   (Bateman et al., 2019).

160   We then focused on SLC transporters and identified 20 SLC transporters, including

161   SLC35D3,   SLC35F1,   and   SLC35G2,   among   the   SV-associated   proteins

162   (Supplementary Table S2). The abundance of these three transporters was similar to

163 known VNTs, including VAChT and the monoamine transporter VMAT2 (Figure 2G),

164 even though VAChT was below the threshold for significance ($p > 0.05$). Comparing the

165 putative vesicular transporters identified in our localization screen with the SLC

166 transporters identified in the SV proteome revealed a total of seven transporters

167 present in both datasets, including the three SLC35 family members (i.e., SLC35D3,

168 SLC35F1, and SLC35G2) identified above (Figure 2H). The other four transporters

169 were previously reported to localize to SVs including the choline transporter SLC5A7

170 (Ferguson et al., 2003; Nakata et al., 2004; Ribeiro et al., 2003), the proline transporter

171 SLC6A7 (Crump et al., 1999; Renick et al., 1999), the neutral amino acid transporter

172 SLC6A17 (Fischer et al., 1999; Masson et al., 1999), and the zinc transporter

173 SLC30A3 (Wenzel et al., 1997).

174

175 ***Localization of SLC35D3 to SVs revealed by EM***

176 To further verify the vesicular localization of one of the three SLC35 candidates,

177 SLC35D3, we used APEX2-based labeling (Lam et al., 2015) coupled with EM (Figure

178 3A). We first validated this strategy by transfecting cultured rat neurons with Mito-

179 APEX2 to label mitochondria and found two distinct populations based on electron

180 density (Figure 3B); as an additional control, we found only one population of SVs in

181 non-transfected neurons (Figure 3C). Importantly, neurons transfected with either

182 VGLUT1-APEX2 (Figure 3D) or SLC35D3-APEX2 (Figure 3E) had two distinct

183 populations of SVs based on electron density, demonstrating that SLC35D3 localizes

184 to SVs in cultured neurons.

185

Deorphanization of SLC35D3 using metabolite profiling combined with a radiolabeled substrate transport assay

188 To search for the cognate substrate corresponding to the orphan vesicular transporter

189 SLC35D3, we used metabolite profiling, based on the assumption that overexpressing

190 the transporter will enrich its cognate substrate in organelles. In our analysis, we

191 intentionally focused on nucleotide sugars present in mammals as possible substrates,

192 as the SLC35 transporter family has been reported to transport these molecules

193 (Figure 4A) (Caffaro and Hirschberg, 2006; Ishida and Kawakita, 2004; Song, 2013).

194 By optimizing a hyperPGC column–based HPLC strategy coupled with selected

195 reaction monitoring in MS (Garcia et al., 2013), we successfully detected a range of

196 nucleotide sugars (Figure 4B). Next, we used the deorphanization strategy shown in

197 Figure 4C. Firstly, we measured nucleotide sugars in untransfected control cells,

198 finding all known nucleotide sugars (Figure 4D,E). To test the sensitivity of this

199 deorphanization strategy, we generated a stable cell line overexpressing EGFP-

200 tagged SLC35A2 (Supplementary Figure S2A), which is known to transport the

201 nucleotide sugars including UDP-galactose and UDP-*N*-acetyl-galactosamine (Ishida

202 et al., 1996; Segawa et al., 2002; Sun-Wada et al., 1998). Profiling the relative

203 abundance of specific nucleotide sugars in organelles prepared from control cells and

204 SLC35A2-overexpressing (SLC35A2OE) cells revealed a >100% increase in the

205 substrate UDP-galactose in SLC35A2OE organelles (Figure 4F,G and Supplementary

206 Figure S2B). Interestingly, we also detected 60% higher levels of both UDP-glucose

207   and UDP-glucuronic acid in SLC35A2OE cells, indicating two previously unknown

208   substrates of the SLC35A2 transporter; in contrast, we found that the SLC35A2

209   substrate UDP-*N*-acetyl-galactosamine did not appear to be enriched in SLC35A2OE

210   cells, possibly due to limitations in separating UDP-*N*-acetyl-glucosamine and UDP-

211   *N*-acetyl-galactosamine in our HPLC-MS setup (Figure 4F,G). We then used this same

212   strategy to search for substrates of the orphan vesicular transporter SLC35D3 using

213   SLC35D3-overexpressing (SLC35D3OE) cells (Supplementary Figure S2A). Our

214   analysis revealed a 40% increase in UDP-glucose and a 30% increase in CMP-sialic

215   acid in SLC35D3OE organelles compared to control organelles (Figure 4H,I and

216   Supplementary Figure S2B), suggesting that these two nucleotide sugars might be

217   substrates of the SLC35D3 transporter.

218   Metabolite profiling can detect the effects of both direct transport activity and

219   indirect changes in the abundance of metabolites due to the overexpression of

220   transporters; thus, we also conducted an uptake assay with radiolabeled nucleotide

221   sugars in order to measure the transport activity (Figure 5A). We found that cells

222   expressing the SLC35A2 transporter had significantly increased uptake of both the

223   previously known substrate UDP-galactose and the newly identified substrate UDP-

224   glucose compared to control cells (Figure 5B), validating our deorphanization strategy

225   combining metabolite profiling and the radiolabeled transport assay. Importantly, cells

226   expressing human SLC35D3 had a nearly 1-fold increase in UDP-glucose transport,

227   but no significant change in the transport of UDP-galactose or UDP-N-acetyl-

228   glucosamine; similar results were obtained from the cells expressed the mouse

229   SLC35D3 (Figure 5B). Thus, UDP-glucose is a promising substrate of SLC35D3.

230

231   ***Characterization of the transport properties of SLC35D3***

232   Next, we characterized the transport of UDP-glucose by SLC35D3. To study the

233   substrate specificity of SLC35D3, we performed a competition assay in which we

234   applied a 100-fold higher concentration of non-radiolabeled substrate together with

235   radiolabeled UDP-glucose in the transport assay. We found that non-radiolabeled

236   UDP-glucose—but not the structurally similar UDP-*N*-acetyl-galactosamine—virtually

237   eliminated the transport of radiolabeled UDP-glucose (Figure 5C). In addition, several

238   other UDP-sugars partially inhibited transport activity, possibly by competing with

239   UDP-glucose on the transporter's substrate-binding pocket. Interestingly, CMP-sialic

240   acid did not reduce the transport of UDP-glucose (Figure 5C), even though this

241   nucleotide sugar was increased—albeit to a lesser extent than UDP-glucose—in the

242   organelles of cells expressing SLC35D3 (see Figure 4I), indicating that CMP-sialic

243   acid may not be a direct substrate of SLC35D3 but may have been indirectly increased

244   on its abundance as shown by metabolite profiling.

245   We also measured the time course and dose dependence of UDP-glucose

246   transport by SLC35D3, revealing a time constant of 2.9 min (Figure 5D) and a Km

247   value of 0.87 µM (Figure 5E). Lastly, we examined the role of the electrochemical

248   proton gradient on SLC35D3 activity, as this gradient has been reported to drive the

249   activity of known VNTs (Edwards, 2007; Van Liefferinge et al., 2013). We therefore

250   applied a variety of pharmacological inhibitors and measured UDP-glucose transport

251 by SLC35D3 (Figure 5F). We found that *N*-ethylmaleimide (NEM), FCCP (carbonyl

252 cyanide-4-(trifluoromethoxy) phenylhydrazone), and nigericin significantly reduced

253 UDP-glucose transport in SLC35D3-expressing cells (Figure 5G), suggesting that the

254 electrochemical proton gradient contributes—at least in part—to the driving force.

255 Taken together, these data support the notion that SLC35D3 is a nucleotide sugar

256 transporter, with UDP-glucose as its primary substrate.

257

258 **Discussion**

259 Here, we report the identification and characterization of three novel SLC35

260 transporters localized to SVs using a combination of localization profiling, proteomics

261 profiling, and EM. Using metabolite profiling combined with a radiolabeled substrate

262 transport assay, we also found that one of these novel vesicular transporters—

263 SLC35D3—is a UDP-glucose transporter. These data indicate the existence of a novel

264 neuronal vesicular transporter of the nucleotide sugar UDP-glucose (Figure 6).

265 Our localization screening strategy revealed a series of vesicular transporter

266 candidates in neurons, a cell type which has tightly regulated secretory vesicles.

267 However, these transporters may also play a physiological role in regulated secretory

268 organelles such as lysosomes and endosomes in non-neuronal secretory cells.

269 It is important to note that some VNTs may have been below the detection limit of

270 enriched proteins in our SV proteomics approach. For example, the vesicular

271 nucleotide transporter SLC17A9 has been reported to play a role in vesicular ATP

272 release (Sawada et al., 2008), but was not identified in our proteomics analyses of

273 SVs, consistent with reports by other groups (Gronborg et al., 2010; Takamori et al.,

274 2006). Similarly, our analysis did not identify SLC10A4, another vesicular transporter

275 (Larhammar et al., 2014). Therefore, studies regarding these low-abundance

276 transporters may require more robust strategies such as enriching specific SVs from

277 VNT-expressing brain regions, using specific antibodies against VNTs, or generating

278 transgenic mice expressing biochemical labels on specific VNTs.

279 Combining metabolite profiling with a radiolabeled substrate transport assay is a

280 powerful tool for identifying and characterizing transporter substrates (Nguyen et al.,

281 2014; Vu et al., 2017), Here, we show that this strategy can indeed be effective for

282 studying orphan vesicular transporters located on secretory organelles.

283 SLC35D3 is expressed primarily in striatal neurons that project to the substantia

284 nigra and the globus pallidus externa in the brain (Lobo et al., 2006), and mice with a

285 recessive mutation in the *SLC35D3* gene have decreased motor activity, impaired

286 energy expenditure, and develop obesity (Zhang et al., 2014). Thus, an important

287 question for future studies is how SLC35D3 and its substrate UDP-glucose play a role

288 in these circuits.

289 Interestingly, previous studies regarding G protein–coupled receptors (GPCRs)

290 found that UDP-sugars, including UDP-glucose, could serve as the ligand of the

291 purinergic receptor P2Y14 (Chambers et al., 2000; Freeman et al., 2001), indicating

292 that nucleotide sugars may function as extracellular signaling molecules, a notion

293 supported by the fact that the P2Y14 receptor is widely expressed in a variety of brain

294 regions and cell types (Chambers et al., 2000; Lee et al., 2003; Zeisel et al., 2018).

295   The P2Y14 receptor is coupled primarily to the Gαi protein (Chambers et al., 2000;

296   Inoue et al., 2019), which does not elicit an excitatory downstream calcium signal.

297   Thus, whether the P2Y14 receptor plays a role in SLC35D3-expressing neurons is an

298   interesting question that warrants investigation.

299

300   **Methods**

301   ***Animals***

302   Postnatal 0-day-old (P0) Sprague-Dawley rats (Beijing Vital River Laboratory) and

303   adult (P42-56) wild-type C57BL/6J (Beijing Vital River Laboratory) were used in this

304   study. All animals were raised in a temperature-controlled room with a 12h/12h light-

305   dark cycle, and all animal procedures were performed using protocols approved by

306   the Animal Care and Use Committees at Peking University.

307

308   ***Molecular biology***

309   DNA fragments were cloned using PCR amplification with primers (TsingKe Biological

310   Technology) containing 30 bp of overlap. The fragments were then assembled into

311   plasmids using Gibson assembly (Gibson et al., 2009). All plasmid sequences were

312   verified using Sanger sequencing (TsingKe Biological Technology). For the localization

313   studies in cultured neurons, the open-reading frames (e.g., SLC-mCherry, SLC-

314   APEX2, SYP-EGFP, organelle marker-EGFP, etc.) were cloned into the N3 vector

315   under the control of the CAG promoter. To generate stable cell lines expressing various

316   SLC35 transporters, we generated the pPacific vector containing a 3' terminal repeat,

317   the CAG promoter, a P2A sequence, the *puromycin* gene, and a 5' terminal repeat;

318   the genes of interest were then cloned into a modified pPiggyBac (namely pPacific)

319   vector using Gibson assembly. Two mutations (S103P and S509G) were introduced in

320   pCS7-PiggyBAC (ViewSolid Biotech) to generate a hyperactive piggyBac transposase

321   for generating the stable cell lines.

322

323   ***Preparation and fluorescence imaging of cultured cells***

324   HEK293T cells were cultured at 37°C in 5% CO_2 in DMEM (Gibco) supplemented with

325   10% (v/v) fetal bovine serum (Gibco) and 1% penicillin-streptomycin (Gibco). For

326   transfection, cells in 6-well plates were incubated in a mixture containing 1 µg DNA

327   and 3 µg PEI for 6 h, and fluorescence imaging was performed after the generation of

328   a stable cell line.

329   Rat cortical neurons were prepared from P0 Sprague-Dawley rat pups (Beijing Vital

330   River Laboratory). In brief, cortical neurons were dissociated from dissected rat brains

331   in 0.25% trypsin-EDTA (GIBCO), plated on 12-mm glass coverslips coated with poly-

332   D-lysine (Sigma-Aldrich), and cultured at 37°C in 5% CO_2 in Neurobasal medium

333   (Gibco) containing 2% B-27 supplement (Gibco), 1% GlutaMAX (Gibco), and 1%

334   penicillin-streptomycin (Gibco). After 7-9 days in culture, the neurons were transfected

335   with SLC-mCherry, SYP-EGFP, organelle markers, or SLC-APEX2, and fluorescence

336   imaging was performed 2-4 days after transfection.

337   Cultured cells were imaged using an inverted Ti-E A1 confocal microscope (Nikon)

338   equipped with a 40×/1.35 NA oil-immersion objective, a 488-nm laser, and a 561-nm

339   laser. During fluorescence imaging, the cells were either bathed or perfused in a

340   chamber containing Tyrode's solution consisting of (in mM): 150 mM NaCl, 4 mM KCl,

341   2 mM $MgCl_2$, 2 mM $CaCl_2$, 10 mM HEPES, and 10 mM glucose (pH 7.4).

342   Localization imaging data of SLC-mCherry fluorescence overlapping with SYP-

343   EGFP puncta were firstly manually selected by three researchers in a double-blind

344   fashion. The selected SLC-mCherry images were further quantified to obtain a co-

345   localization ratio with SYP-EGFP using the modified *in silica* Puncta Analyzer tool, as

346   described previously (Kimura et al., 2007).

347

348   ***Western blot***

349   Protein lysates were denatured by the addition of 2x sample buffer followed by 70°C

350   treatment for 10 min. Samples were resolved by 10% SDS-PAGE, transferred for 1 hr

351   at room temperature at 25 V to NC membranes, and analyzed by immunoblotting.

352   Membranes were firstly stained by Ponceau S staining followed by washing with TBST

353   and blocking with 5% non-fat milk prepared in TBST for 1 hr at room temperature.

354   Membranes were then incubated with primary antibodies in 5% non-fat milk TBST

355   overnight at 4°C, followed by washing with TBST three times, 10 min each.

356   Membranes were incubated with the corresponding secondary antibodies in 5% non-

357   fat milk for 2 hr at room temperature. Membranes were then washed three more times,

358   10 min each, with TBST before being visualized using chemiluminescence. Antibodies

359   used were polyclonal rabbit anti-VGLUT1 (135302; Synaptic Systems), polyclonal

360   rabbit anti-VGLUT2 (135402; Synaptic Systems), monoclonal mouse anti-SYP

361 (101011; Synaptic Systems), polyclonal rabbit anti-SYP (5461; Cell Signaling

362 Technology), monoclonal mouse anti-VAMP2 (104211; Synaptic Systems),

363 monoclonal mouse anti-PSD95 (75-028; NeuroMab).

364

365 ***Proteomics analysis of SVs***

366 Thirty minutes prior to use, 5 µg of antibody was conjugated to 50 µl Protein G M-280

367 dynabeads at room temperature in KPBS buffer containing (in mM): 136 KCl and 10

368 KH_2PO_4 (pH 7.25). The brain was removed from an adult (P42-56) C57BL/6J mouse,

369 homogenized using a ball-bearing homogenizer (10-µm clearance) in 3 ml ice-cold

370 KPBS, and centrifuged at 30,000g for 20 min. The supernatant (input) containing the

371 SVs was collected and incubated with antibody-conjugated dynabeads for 1 hr at 0°C

372 for immunoisolation. Dynabead-bound SVs were washed 3 times with KPBS and

373 eluted by incubating the samples with SDS-PAGE sample loading buffer. The SV

374 samples were heated for 10 min at 70°C, centrifuged for 2 min at 14,000 rpm, and the

375 supernatants were transferred to clean tubes. The protein samples were then

376 subjected to SDS-PAGE for western blotting and HPLC-MS, respectively.

377 The resolved proteins in SDS-PAGE were digested and extracted from the gel

378 pieces using acetonitrile containing 0.1% formic acid (FA). The samples were then

379 dried in a vacuum centrifuge concentrator at 30°C and resuspended in 10 µl 0.1% FA.

380 Using an Easy-nLC 1200 system, 5 µl of sample was loaded at a rate of 0.3 µl/min

381 in 0.1% FA onto a trap column (C18, Acclaim PepMap 100 75 um x 2 cm; Thermo

382 Fisher Scientific) and eluted across a fritless analytical resolving column (C18, Acclaim

383   PepMap 75 um x 15 cm; Thermo Fisher Scientific) with a 75-min gradient of 4% to 30%

384   LC-MS buffer B at 300 nl/min; buffer A contained 0.1% FA, and buffer B contained 0.1%

385   FA and 80% acetonitrile.

386   The peptides were directly injected into an Orbitrap Fusion Lumos (Thermo Fisher

387   Scientific) using a nano-electrospray ion source with an electrospray voltage of 2.2 kV.

388   Full scan MS spectra were acquired using the Orbitrap mass analyzer (m/z range:

389   300–1500 Da) with the resolution set to 60,000 (full width at half maximum, or FWHM)

390   at m/z = 200 Da. Full scan target was 5e5 with a maximum fill time of 50 ms. All data

391   were acquired in profile mode using positive polarity. MS/MS spectra data were

392   acquired using Orbitrap with a resolution of 15,000 (FWHM) at m/z = 200 Da and

393   higher-collisional dissociation (HCD) MS/MS fragmentation. The isolation width was

394   1.6 m/z.

395

396   ***Electron microscopy***

397   Antibody conjugated dynabeads were pelleted by centrifugation and subsequently

398   resuspended in 1.5% agarose in 0.1 M phosphate buffer (PB, pH 7.4). Small agarose

399   blocks were cut out, fixed overnight at 4°C using 4% glutaraldehyde in 0.1 M PB at pH

400   7.4, followed by post-fixation of 1% osmium tetroxide for 1 hr and treatment of 0.25%

401   uranyl acetate overnight at 4°C. The samples were then dehydrated in a graded

402   ethanol series (20%, 50%, 70%, 80%, 90%, 95%, 100%, 100%) at 8 min per step and

403   then changed to propylene oxide for 10min. The cells were then infiltrated in Epon 812

404   resin using a 1:1 ratio of propylene oxide and resin for 4hr, followed by 100% resin

405 twice at 4 hr each; finally, the beads were placed in fresh resin and polymerized in a

406 vacuum oven at 65°C for 24 hr. After polymerization, ultrathin sections were cut and

407 stained with lead citrate.

408 For APEX2 based EM labeling, the procedure was adapted from previous study

409 (Martell et al., 2012). Transfected neurons were firstly fixed with 2% glutaraldehyde in

410 0.1 M PB at room temperature, quickly placed on ice, and incubated on ice for 45-60

411 min. The cells were rinsed with chilled PB twice at 5 min each before adding 20 mM

412 glycine to quench any unreacted glutaraldehyde. The cells were then rinsed three

413 times with PB at 5 min each. Freshly prepared solution containing 0.5 mg/ml 3,3′-

414 diaminobenzidine (DAB) tetrahydrochloride and 10 mM H_2O_2 was then added to the

415 cells. After 5-10 min, the reaction was stopped by removing the DAB solution and

416 rinsing three times with chilled PB at 5 min each. The cells were then incubated in 2%

417 osmium tetroxide in 0.1 M PB combined with 0.1 M imidazole (pH 8.0) for 30 min in a

418 light-proof box. The cells were then rinsed six times with water at 5 min each and then

419 incubated in 2% (w/v) aqueous uranyl acetate overnight at 4°C. The cells were rinsed

420 six times with water at 5 min each, and then dehydrated in a graded ethanol series

421 (20%, 50%, 70%, 80%, 90%, 95%, 100%, 100%) at 8 min per step, and then rinsed

422 once in anhydrous ethanol at room temperature. The cells were then infiltrated in Epon

423 812 resin using a 1:1, 1:2, and 1:3 (v/v) ratio of anhydrous ethanol and resin for 1 hr,

424 2 hr, and 4 hr, respectively, followed by 100% resin twice at 4 hr each; finally, the cells

425 were placed in fresh resin and polymerized in a vacuum oven at 65°C for 24 hr.

426 The embedded cells were cut into 60-nm ultrathin sections using a diamond knife

427 and imaged using a FEI-Tecnai G2 20 TWIN transmission electron microscope

428 operated at 120 KV.

429

430 ***Organelle fractionation***

431 Stable cell lines grown in two 15-cm dishes were washed twice with either ice-cold

432 KPBS (for metabolite detection) or sucrose buffer containing 0.32 M sucrose and 4

433 mM HEPES-NaOH (pH 7.4) (for the uptake assay), and then gently scraped and

434 collected into 1 ml of the corresponding buffer. The cells were then homogenized using

435 a ball-bearing homogenizer (10-μm clearance). The homogenate was centrifuged at

436 13,000*g* for 10 min to remove the nuclei and cellular debris. The resulting supernatant

437 was centrifuged at 200,000*g* for 25 min. For metabolite profiling, the pellet was washed

438 3 times in ice-cold KPBS, and the metabolites were extracted in 80% methanol, freeze-

439 dried, and stored at -80°C. For the transport assay, the pellet was resuspended in

440 uptake assay buffer containing 0.32 M sucrose, 2 mM KCl, 2 mM NaCl, 4 mM $MgSO_4$,

441 and 10 mM HEPES-KOH (pH 7.4), aliquoted, and stored at -80°C.

442

443 ***Targeted metabolite profiling***

444 Samples were analyzed using a TSQ Quantiva Ultra triple-quadrupole mass

445 spectrometer coupled with an Ultimate 3000 UPLC system (Thermo Fisher Scientific)

446 equipped with a heated electrospray ionization probe. Chromatographic separation

447 was achieved using gradient elution on a Hypercarb PGC column (2.1 × 100 mm, 1.7

448 μm, Thermo Fisher Scientific). Mobile phase A consisted of 5 mM ammonium

449 bicarbonate dissolved in pure water, and mobile phase B consisted of 100%

450 acetonitrile. A 25-minute gradient with a flow rate of 250 μl/min was applied as follows:

451 0-1.2 min, 4% B; 1.2-19 min, 4-35% B; 19-20 min, 35-98% B; 20-22 min, 98% B; 22-

452 25 min 4% B. The column chamber and sample tray were kept at 45°C and 10°C,

453 respectively. Data were acquired using selected reaction monitoring in negative switch

454 ion mode, and optimal transitions are reported as the reference. Both the precursor

455 and fragment ion fractions were collected at a resolution of 0.7 FWHM. The source

456 parameters were as follows: spray voltage: 3000 V; ion transfer tube temperature:

457 350°C; vaporizer temperature: 300°C; sheath gas flow rate: 35 arbitrary units; auxiliary

458 gas flow rate: 12 arbitrary units; collision induced dissociation (CID) gas pressure: 1.5

459 mTorr.

460

461 ***Uptake assay***

462 For the radiolabeled substrate transport assay, 20 μg of the membrane fraction was

463 incubated with the indicated concentration of radiolabeled substrate at 37°C for 5 min

464 (unless otherwise). The reaction was terminated using the same volume of ice-cold

465 assay buffer. The samples were then trapped on a 0.7-μm GF/F glass fiber filter

466 (Whatman) and washed twice. The radioactivity retained on the filter was measured

467 using liquid scintillation.

468

469 ***Quantification and statistical analysis***

470 Imaging data from cultured cells were processed using ImageJ software (NIH). SV

471 proteomics data were analyzed using MaxQuant_1.6.10.43 (MPI). The metabolite

472 profiling data were analyzed and quantified using Xcalibur version 3.0.63 (Thermo

473 Fisher Scientific). Sequence data for generating the phylogenic tree of were analyzed

474 by MEGA-X. All summary data are presented as the mean ± s.e.m., and group data

475 were compared using the Student's *t*-test; *$p < 0.05$, **$p < 0.01$, ***$p < 0.001$, and n.s., not

476 significant ($p > 0.05$).

477

478 ***Data and software availability***

479 The custom-written programs will be provided upon request to the corresponding

480 author, Yulong Li (yulongli@pku.edu.cn).

481

482 **Acknowledgments**

492

Author contributions

Y.L. and Y. R. supervised the project. C.Q., Z.W., R.S., H.Y., and J.Z. designed and performed the localization screen of SLCs in cultured neurons. Z.W. designed and performed the immunoisolation of SVs and western blotting. C.Q. designed and performed the SV proteomics analysis. R.S. designed and performed electron microscopy experiments. C.Q. designed and performed the deorphanization of SLC35 experiments. All authors contributed to the data interpretation and analysis. C.Q. and Y.L. wrote the manuscript with input from all other authors.

References

Andersen, J.S., Wilkinson, C.J., Mayor, T., Mortensen, P., Nigg, E.A., and Mann, M. (2003). Proteomic characterization of the human centrosome by protein correlation profiling. Nature *426*, 570-574.

Bateman, A., Martin, M.J., Orchard, S., Magrane, M., Alpi, E., Bely, B., Bingley, M., Britto, R., Bursteinas, B., Busiello, G.*, et al.* (2019). UniProt: a worldwide hub of protein knowledge. Nucleic Acids Res *47*, D506-D515.

Blakely, R.D., and Edwards, R.H. (2012). Vesicular and Plasma Membrane Transporters for Neurotransmitters. Csh Perspect Biol *4*.

Boyken, J., Gronborg, M., Riedel, D., Urlaub, H., Jahn, R., and Chua, J.J.E. (2013). Molecular Profiling of Synaptic Vesicle Docking Sites Reveals Novel Proteins but Few Differences between Glutamatergic and GABAergic Synapses. Neuron *78*, 285-297.

Burgoyne, R.D., and Morgan, A. (2003). Secretory granule exocytosis. Physiological reviews *83*, 581-632.

Caffaro, C.E., and Hirschberg, C.B. (2006). Nucleotide sugar transporters of the golgi apparatus: From basic science to diseases. Accounts Chem Res *39*, 805-812.

Cesar-Razquin, A., Snijder, B., Frappier-Brinton, T., Isserlin, R., Gyimesi, G., Bai, X.Y., Reithmeier, R.A., Hepworth, D., Hediger, M.A., Edwards, A.M.*, et al.* (2015). A Call for Systematic Research on Solute Carriers. Cell *162*, 478-487.

Chambers, J.K., Macdonald, L.E., Sarau, H.M., Ames, R.S., Freeman, K., Foley, J.J., Zhu, Y., McLaughlin, M.M., Murdock, P., McMillan, L.*, et al.* (2000). A G protein-coupled receptor for UDP-glucose. Journal of Biological Chemistry *275*, 10767-10771.

Chantranupong, L., Saulnier, J.L., Wang, W.G., Jones, D.R., Pacold, M.E., and Sabatini, B.L. (2020). Rapid purification and metabolomic profiling of synaptic vesicles from mammalian brain. Elife *9*.

Chong, Y.T., Koh, J.L.Y., Friesen, H., Duffy, K., Cox, M.J., Moses, A., Moffat, J., Boone, C., and Andrews, B.J. (2015). Yeast Proteome Dynamics from Single Cell Imaging and Automated Analysis. Cell *161*, 1413-1424.

Christoforou, A., Mulvey, C.M., Breckels, L.M., Geladaki, A., Hurrell, T., Hayward, P.C., Naake, T., Gatto, L., Viner, R., Arias, A.M.*, et al.* (2016). A draft map of the mouse pluripotent stem cell spatial proteome. Nature

527   Communications *7*.

528   Crump, F.T., Fremeau, R.T., and Craig, A.M. (1999). Localization of the brain-specific high-affinity L-proline
529   transporter in cultured hippocampal neurons: Molecular heterogeneity of synaptic terminals. Mol Cell Neurosci
530   *13*, 25-39.

531   Edwards, R.H. (2007). The neurotransmitter cycle and quantal size. Neuron *55*, 835-858.

532   Ferguson, S.M., Savchenko, V., Apparsundaram, S., Zwick, M., Wright, J., Heilman, C.J., Yi, H., Levey, A.I., and
533   Blakely, R.D. (2003). Vesicular localization and activity-dependent trafficking of presynaptic choline transporters.
534   Journal of Neuroscience *23*, 9697-9709.

535   Fernandez-Suarez, M., and Ting, A.Y. (2008). Fluorescent probes for super-resolution imaging in living cells.
536   Nature Reviews Molecular Cell Biology *9*, 929-943.

537   Fischer, J., Bancila, V., Mailly, P., Masson, J., Hamon, M., El Mestikawy, S., and Conrath, M. (1999).
538   Immunocytochemical evidence of vesicular localization of the orphan transporter Rxt1 in the rat spinal cord.
539   Neuroscience *92*, 729-743.

540   Freeman, K., Tsui, P., Moore, D., Emson, P.C., Vawter, L., Naheed, S., Lane, P., Bawagan, H., Herrity, N., Murphy, K.*,
541   et al.* (2001). Cloning, pharmacology, and tissue distribution of G-protein-coupled receptor GPR105 (KIAA0001)
542   rodent orthologs. Genomics *78*, 124-128.

543   Garcia, A.D., Chavez, J.L., and Mechref, Y. (2013). Sugar nucleotide quantification using multiple reaction
544   monitoring liquid chromatography/tandem mass spectrometry. Rapid Commun Mass Sp *27*, 1794-1800.

545   Gibson, D.G., Young, L., Chuang, R.Y., Venter, J.C., Hutchison, C.A., 3rd, and Smith, H.O. (2009). Enzymatic
546   assembly of DNA molecules up to several hundred kilobases. Nat Methods *6*, 343-345.

547   Gronborg, M., Pavlos, N.J., Brunk, I., Chua, J.J.E., Munster-Wandowski, A., Riedel, D., Ahnert-Hilger, G., Urlaub,
548   H., and Jahn, R. (2010). Quantitative Comparison of Glutamatergic and GABAergic Synaptic Vesicles Unveils
549   Selectivity for Few Proteins Including MAL2, a Novel Synaptic Vesicle Protein. Journal of Neuroscience *30*, 2-12.

550   Hediger, M.A., Clemencon, B., Burrier, R.E., and Bruford, E.A. (2013). The ABCs of membrane transporters in
551   health and disease (SLC series): Introduction. Molecular Aspects of Medicine *34*, 95-107.

552   Huh, W.K., Falvo, J.V., Gerke, L.C., Carroll, A.S., Howson, R.W., Weissman, J.S., and O'Shea, E.K. (2003). Global
553   analysis of protein localization in budding yeast. Nature *425*, 686-691.

554   Inoue, A., Raimondi, F., Kadji, F.M.N., Singh, G., Kishi, T., Uwamizu, A., Ono, Y., Shinjo, Y., Ishida, S., Arang, N.*, et
555   al.* (2019). Illuminating G-Protein-Coupling Selectivity of GPCRs. Cell *177*, 1933-+.

556   Ishida, N., and Kawakita, M. (2004). Molecular physiology and pathology of the nucleotide sugar transporter
557   family (SLC35). Pflug Arch Eur J Phy *447*, 768-775.

558   Ishida, N., Miura, N., Yoshioka, S., and Kawakita, M. (1996). Molecular cloning and characterization of a novel
559   isoform of the human UDP-galactose transporter, and of related complementary DNAs belonging to the
560   nucleotide-sugar transporter gene family. Journal of Biochemistry *120*, 1074-1078.

561   Itzhak, D.N., Tyanova, S., Cox, J., and Borner, G.H.H. (2016). Global, quantitative and dynamic mapping of protein
562   subcellular localization. Elife *5*.

563   Kimura, S., Noda, T., and Yoshimori, T. (2007). Dissection of the autophagosome maturation process by a novel
564   reporter protein, tandem fluorescent-tagged LC3. Autophagy *3*, 452-460.

565   Koopmans, F., van Nierop, P., Andres-Alonso, M., Bymes, A., Cijsouw, T., Coba, M.P., Cornelisse, L.N., Farrell, R.J.,
566   Goldschmidt, H.L., Howrigan, D.P.*, et al.* (2019). SynGO: An Evidence-Based, Expert-Curated Knowledge Base for
567   the Synapse. Neuron *103*, 217-+.

568   Kreda, S., Seminario–Vidal, L., Heusden, C.v., and Lazarowski, E. (2008). Thrombin–promoted release of UDP–
569   glucose from human astrocytoma cells. British journal of pharmacology *153*, 1528-1537.

570   Laek, M., Weingarten, J., and Volknandt, W. (2015). The synaptic proteome. Cell Tissue Res *359*, 255-265.

571   Lam, S.S., Martell, J.D., Kamer, K.J., Deerinck, T.J., Ellisman, M.H., Mootha, V.K., and Ting, A.Y. (2015). Directed
572   evolution of APEX2 for electron microscopy and proximity labeling. Nature methods *12*, 51-54.

573   Larhammar, M., Patra, K., Blunder, M., Emilsson, L., Peuckert, C., Arvidsson, E., Rönnlund, D., Preobraschenski, J.,
574   Birgner, C., and Limbach, C. (2014). SLC10A4 is a vesicular amine-associated transporter modulating dopamine
575   homeostasis. Biological psychiatry.

576   Lazarowski, E.R., Shea, D.A., Boucher, R.C., and Harden, T.K. (2003). Release of cellular UDP-glucose as a potential
577   extracellular signaling molecule. Mol Pharmacol *63*, 1190-1197.

578   Lee, B.C., Cheng, T., Adams, G.B., Attar, E.C., Miura, N., Lee, S.B., Saito, Y., Olszak, I., Dombkowski, D., Olson, D.P*.,
579   et al.* (2003). P2Y-like receptor, GPR105 (P2Y14), identifies and mediates chemotaxis of bone-marrow
580   hematopoietic stem cells. Genes Dev *17*, 1592-1604.

581   Lobo, M.K., Karsten, S.L., Gray, M., Geschwind, D.H., and Yang, X.W. (2006). FACS-array profiling of striatal
582   projection neuron subtypes in juvenile and adult mouse brains. Nature neuroscience *9*, 443-452.

583   Martell, J.D., Deerinck, T.J., Sancak, Y., Poulos, T.L., Mootha, V.K., Sosinsky, G.E., Ellisman, M.H., and Ting, A.Y.
584   (2012). Engineered ascorbate peroxidase as a genetically encoded reporter for electron microscopy. Nature
585   Biotechnology *30*, 1143-+.

586   Masson, J., Riad, M., Chaudhry, F., Darmon, M., Aidouni, Z., Conrath, M., Giros, B., Hamon, M., Storm-Mathisen,
587   J., Descarries, L*., et al.* (1999). Unexpected localization of the Na+/Cl--dependent-like orphan transporter, Rxt1,
588   on synaptic vesicles in the rat central nervous system. Eur J Neurosci *11*, 1349-1361.

589   Moremen, K.W., Tiemeyer, M., and Nairn, A.V. (2012). Vertebrate protein glycosylation: diversity, synthesis and
590   function. Nature Reviews Molecular Cell Biology *13*, 448-462.

591   Nakata, K., Okuda, T., and Misawa, H. (2004). Ultrastructural localization of high-affinity choline transporter in
592   the rat neuromuscular junction: Enrichment on synaptic vesicles. Synapse *53*, 53-56.

593   Nguyen, L.N., Ma, D.L., Shui, G.H., Wong, P.Y., Cazenave-Gassiot, A., Zhang, X.D., Wenk, M.R., Goh, E.L.K., and
594   Silver, D.L. (2014). Mfsd2a is a transporter for the essential omega-3 fatty acid docosahexaenoic acid. Nature *509*,
595   503-+.

596   Orre, L.M., Vesterlund, M., Pan, Y.B., Arslan, T., Zhu, Y.F., Woodbridge, A.F., Frings, O., Fredlund, E., and Lehtio, J.
597   (2019). SubCellBarCode: Proteome-wide Mapping of Protein Localization and Relocalization. Mol Cell *73*, 166-+.

598   Perland, E., and Fredriksson, R. (2017). Classification Systems of Secondary Active Transporters. Trends in
599   Pharmacological Sciences *38*, 305-315.

600   Renick, S.E., Kleven, D.T., Chan, J., Stenius, K., Milner, T.A., Pickel, V.M., and Fremeau, R.T. (1999). The mammalian
601   brain high-affinity L-proline transporter is enriched preferentially in synaptic vesicles in a subpopulation of
602   excitatory nerve terminals in rat forebrain. Journal of Neuroscience *19*, 21-33.

603   Ribeiro, F.M., Alves-Silva, J., Volknandt, W., Martins-Silva, C., Mahmud, H., Wilhelm, A., Gomez, M.V., Rylett, R.J.,
604   Ferguson, S.S.G., Prado, V.F*., et al.* (2003). The hemicholinium-3 sensitive high affinity choline transporter is
605   internalized by clathrin-mediated endocytosis and is present in endosomes and synaptic vesicles. J Neurochem
606   *87*, 136-146.

607   Sawada, K., Echigo, N., Juge, N., Miyaji, T., Otsuka, M., Omote, H., Yamamoto, A., and Moriyama, Y. (2008).
608   Identification of a vesicular nucleotide transporter. Proceedings of the National Academy of Sciences *105*, 5683-
609   5686.

610   Segawa, H., Kawakita, M., and Ishida, N. (2002). Human and Drosophila UDP-galactose transporters transport
611   UDP-N-acetylgalactosamine in addition to UDP-galactose. Eur J Biochem *269*, 128-138.

612   Sesma, J.I., Esther, C.R., Kreda, S.M., Jones, L., O'Neal, W., Nishihara, S., Nicholas, R.A., and Lazarowski, E.R. (2009).
613   Endoplasmic reticulum/golgi nucleotide sugar transporters contribute to the cellular release of UDP-sugar
614   signaling molecules. Journal of Biological Chemistry *284*, 12572-12583.

615   Simpson, J.C., Wellenreuther, R., Poustka, A., Pepperkok, R., and Wiemann, S. (2000). Systematic subcellular
616   localization of novel proteins identified by large-scale cDNA sequencing. Embo Rep *1*, 287-292.
617   Song, Z. (2013). Roles of the nucleotide sugar transporters (SLC35 family) in health and disease. Molecular
618   aspects of medicine *34*, 590-600.
619   Sun-Wada, G.H., Yoshioka, S., Ishida, N., and Kawakita, M. (1998). Functional expression of the human UDP-
620   galactose transporters in the yeast Saccharomyces cerevisiae. Journal of Biochemistry *123*, 912-917.
621   Takamori, S., Holt, M., Stenius, K., Lemke, E.A., Gronborg, M., Riedel, D., Urlaub, H., Schenck, S., Brugger, B.,
622   Ringler, P.*, et al.* (2006). Molecular anatomy of a trafficking organelle. Cell *127*, 831-846.
623   Van Liefferinge, J., Massie, A., Portelli, J., Di Giovanni, G., and Smolders, I. (2013). Are vesicular neurotransmitter
624   transporters potential treatment targets for temporal lobe epilepsy? Frontiers in Cellular Neuroscience *7*.
625   Vu, T.M., Ishizu, A.N., Foo, J.C., Toh, X.R., Zhang, F.Y., Whee, D.M., Torta, F., Cazenave-Gassiot, A., Matsumura, T.,
626   Kim, S.*, et al.* (2017). Mfsd2b is essential for the sphingosine-1-phosphate export in erythrocytes and platelets.
627   Nature *550*, 524-+.
628   Wenzel, H.J., Cole, T.B., Born, D.E., Schwartzkroin, P.A., and Palmiter, R.D. (1997). Ultrastructural localization of
629   zinc transporter-3 (ZnT-3) to synaptic vesicle membranes within mossy fiber boutons in the hippocampus of
630   mouse and monkey. Proceedings of the National Academy of Sciences of the United States of America *94*, 12676-
631   12681.
632   Zeisel, A., Hochgerner, H., Lonnerberg, P., Johnsson, A., Memic, F., van der Zwan, J., Haring, M., Braun, E., Borm,
633   L.E., La Manno, G.*, et al.* (2018). Molecular Architecture of the Mouse Nervous System. Cell *174*, 999-+.
634   Zhang, Z., Hao, C.J., Li, C.G., Zang, D.J., Zhao, J., Li, X.N., Wei, A.H., Wei, Z.B., Yang, L., He, X.*, et al.* (2014). Mutation
635   of SLC35D3 Causes Metabolic Syndrome by Impairing Dopamine Signaling in Striatal D1 Neurons. Plos Genet *10*.

636

637

Figure 1. Localization profiling of SLC family members reveals candidate vesicular transporters

(A) Top: Schematic diagram of the localization profiling strategy. Red and green fluorescent signals were collected using confocal microscopy imaging of cultured rat neurons co-expressing mCherry-tagged SLC proteins and EGFP-tagged synaptophysin (SYP-EGFP). Bottom: Sequential steps used for the localization profiling. Two rounds of screening revealed a total of 40 out of 361 screened SLC transporters as candidate vesicular transporters.

(B) Representative images of neurons expressing SLC X-mCherry transporters (red) and SYP-EGFP (green). Scale bars: 10 μm.

(C) Representative images of neurons expressing three known vesicular SLC transporters (red) and SYP-EGFP (green), with magnified views. White arrowheads indicate co-localization. Scale bars: 10 μm.

(D) Representative images of neurons expressing three non-vesicular organelle markers (red) and SYP-EGFP (green), with magnified views. Scale bars: 10 μm.

(E) Summary of the co-localization ratio between 134 proteins and SYP-EGFP. Dark gray bars represent known vesicular transporters, magenta bars represent SLC35 transporters, light gray bars represent non-vesicular organelle markers, and white bars represent the SLC transporters screened in this study. The threshold indicated by the vertical dashed line was defined as the co-localization ratio between VGLUT3 and SYP-EGFP. n = at least 3 neurons each.

(F,G) Representative images of neurons expressing vesicular (F) and non-vesicular

660   (G) SLC35 transporters (red) and SYP-EGFP (green), with magnified views. White

661   arrowheads indicate co-localization. Scale bars: 10 μm.

662

663   **Figure 2. Proteomics profiling of SVs identifies novel putative vesicular SLC**

664   **transporters**

665   (A) Schematic diagram depicting the strategy for proteomics profiling of SVs

666   immunoisolated from fractionated mouse brain homogenates.

667   (B) Top: western blot analysis of the indicated protein markers for SVs and the

668   postsynaptic marker PSD-95 in the input fraction (supernatant after centrifugation of

669   whole brain lysates), the anti-SYP immunoisolated sample, and the control IgG sample.

670   Bottom: Ponceau staining of the membrane, showing the total proteins.

671   (C) Electron microscopy images of anti-SYP beads (top) and control IgG beads

672   (bottom), with magnified views. Arrowheads indicate immunoisolated SVs. Scale bars:

673   500 nm and 100 nm (magnified views). The bottom-left panel shows the quantification

674   of the number of SVs attached to the indicated beads.

675   (D) Left: volcano plot depicting the proteins detected using SV proteomics. The blue

676   dashed box indicates anti-SYP–enriched proteins using thresholds set at $p<0.05$ and

677   LFQ intensity $>2^{20}$. n = 3 biological replicates. Right: magnified view of the anti-SYP–

678   enriched proteins. Representative SV markers are shown in black, V-ATPase subunits

679   are shown in purple, and known vesicular transporters are shown in red.

680   (E) Venn diagram showing the overlap between anti-SYP–enriched proteins (blue) and

681   the known SV proteome based on the SynGO database (red).

(F) Summary of the percentage of overlap between anti-SYP–enriched proteins and the SV proteome (from the SynGO database), Golgi apparatus proteins (from UniProt), mitochondrial proteins (from UniProt), and the entire mouse proteome (from UniProt).

(G) Summary of the SLC transporters identified using SV proteomics. Classic VNTs are shown in red, and SLC35 transporters are shown in magenta. The horizontal dashed line indicates the threshold at p=0.05.

(I) Venn diagram showing the overlap between the vesicular transporters identified using localization profiling (yellow) and the vesicular transporters identified using proteomics profiling of SVs (blue). The three candidate SLC35 transporters are shown in magenta.

Figure 3. Validation of the vesicular localization of SLC35D3 using electron microscopy

(A) Schematic diagram depicting the APEX2-based labeling strategy for studying ultrastructural localization.

(B-E) Representative EM images (left) and distribution of organelle darkness (right) of mitochondria in cultured rat neurons transfected with Mito-APEX2 (B), SVs in non-transfected neurons (C), and SVs in neurons transfected with either VGLUT1-APEX2 (D) or SLC35D3-APEX2 (E), with magnified views of the dashed boxes from panel E. The blue arrows and red arrowheads indicate organelles with low (light) and high (dark) electron density, respectively. Scale bars: 500 nm.

704 **Figure 4. The targeted metabolite profiling reveals putative substrates of**

705 **SLC35D3**

706 (A) Phylogenic tree of the SLC35 transporter family and known corresponding

707 substrates. SLC35A2 and SLC35D3 are shown in blue and green, respectively.

708 (B) Left: representative HPLC-MS trace showing 5 μM of the indicated nucleotide

709 sugars. The inset shows the linear correlation between the UDP-glc standard and MS

710 ion intensity (R^2=0.997). Right: molecular structures of the UDP-sugars UDP-glc,

711 UDP-gal, UDP-glcNAc, and UDP-galNAc, with differences shown in the gray dashed

712 boxes.

713 (C) Schematic diagram depicting the strategy for detecting metabolites in organelles

714 and in whole cells.

715 (D) Representative traces of the indicated nucleotide sugars detected in control

716 (SLC35A2KO) cells, with a magnified view at the right.

717 (E) Summary of the relative abundance of the indicated nucleotide sugars measured

718 in control cells and cells overexpressing SLC35D3. n = 5 and 3 biological samples,

719 respectively.

720 (F-G) Representative extracted ion chromatograms of specific nucleotide sugars (F)

721 and summary of their relative abundance (G) in organelles isolated from control cells

722 (gray) and cells overexpressing SLC35A2 (blue). N.D.: not detectable. n = 3 per group.

723 (H-I) Representative extracted ion chromatograms of specific nucleotide sugars (F)

724 and summary of their relative abundance (G) in organelles isolated from control cells

725 (gray) and cells overexpressing SLC35D3 (green). N.D.: not detectable. n = 3 per

726   group.

727

728   **Figure 5. Validation and characterization of the UDP-glucose transport activity**

729   **of SLC35D3**

730   (A) Schematic diagram depicting the transport assay using organelles isolated from

731   HEK293T cells.

732   (B) Summary of the transport of [^{3}H]-UDP-glc, [^{3}H]-UDP-gal, and [^{3}H]-UDP-glcNAc

733   (500 nM each) in control (SLC35A2KO) cells and in cells overexpressing mouse

734   SLC35D3 (mSLC35D3), human SLC35D3 (hSLC35D3), or human SLC35A2

735   (hSLC35A2); n = 3 experiments each.

736   (C) Competition assay measuring [^{3}H]-UDP-glc (500 nM) transport in the presence of

737   the indicated non-labeled compounds (at 50 µM) in cells expressing SLC35D3; the

738   data are expressed relative to mock cells, in which solvent was applied instead of a

739   non-labeled compound; n = 3 experiments each.

740   (D) Time course of [^{3}H]-UDP-glc transport measured in cells expressing SLC35D3,

741   relative to baseline. The data were fitted to a single-exponential function.

742   (E) Dose-response curve for [^{3}H]-UDP-glc transport in cells expressing SLC35D3,

743   relative to the corresponding baseline values. The data were fitted to Michaelis–

744   Menten kinetics equation.

745   (F) Schematic diagram depicting the proton gradient driving vesicular transporters,

746   with specific inhibitors shown.

747   (G) Summary of [^{3}H]-UDP-glc transport measured in cells expressing SLC35D3,

748   expressed relative to mock cells, in which solvent was applied; n = 3 experiments each.

749   NEM, *N*-ethylmaleimide (0.2 mM); FCCP, carbonyl cyanide-4-(trifluoromethoxy)

750   phenylhydrazone (50µM); Nig, Nigericin (5 µM); Baf, bafilomycin A1 (100 nM); Val,

751   valinomycin (20 µM).

752

753   **Figure 6. Working model depicting SLC35D3 as a UDP-glucose transporter on**

754   **SVs**

755   SLC35D3 is a vesicular transporter which potentially mediate transport of UDP-

756   glucose into SVs. UDP-glucose may function as a signaling molecule through a GPCR

757   namely P2Y14.

758

759   **Supplementary Figure S1. Repeatability of the proteomic data (related to Figure**

760   **2)**

761   Scatterplots showing the correlation between independent biological trials.

762

763   **Supplementary Figure S2. Additional analysis of metabolite profiling (related to**

764   **Figure 4)**

765   (A) Representative brightfield (BF) and fluorescence (GFP) images of control

766   (SLC35A2KO) cells and cells overexpressing EGFP-tagged SLC35A2 (SLC35A2-

767   EGFP) or SLC35D3 (SLC35D3-EGFP). Scale bar: 10 µm.

768   (B) Representative full traces (left) and expanded views (right) of nucleotide sugars

769   detected in organelles isolated from control cells (top) and from cells overexpressing

770   SLC35A2-EGFP (SLC35A2OE) or SLC35D3-EGFP (SLC35D3OE).

771
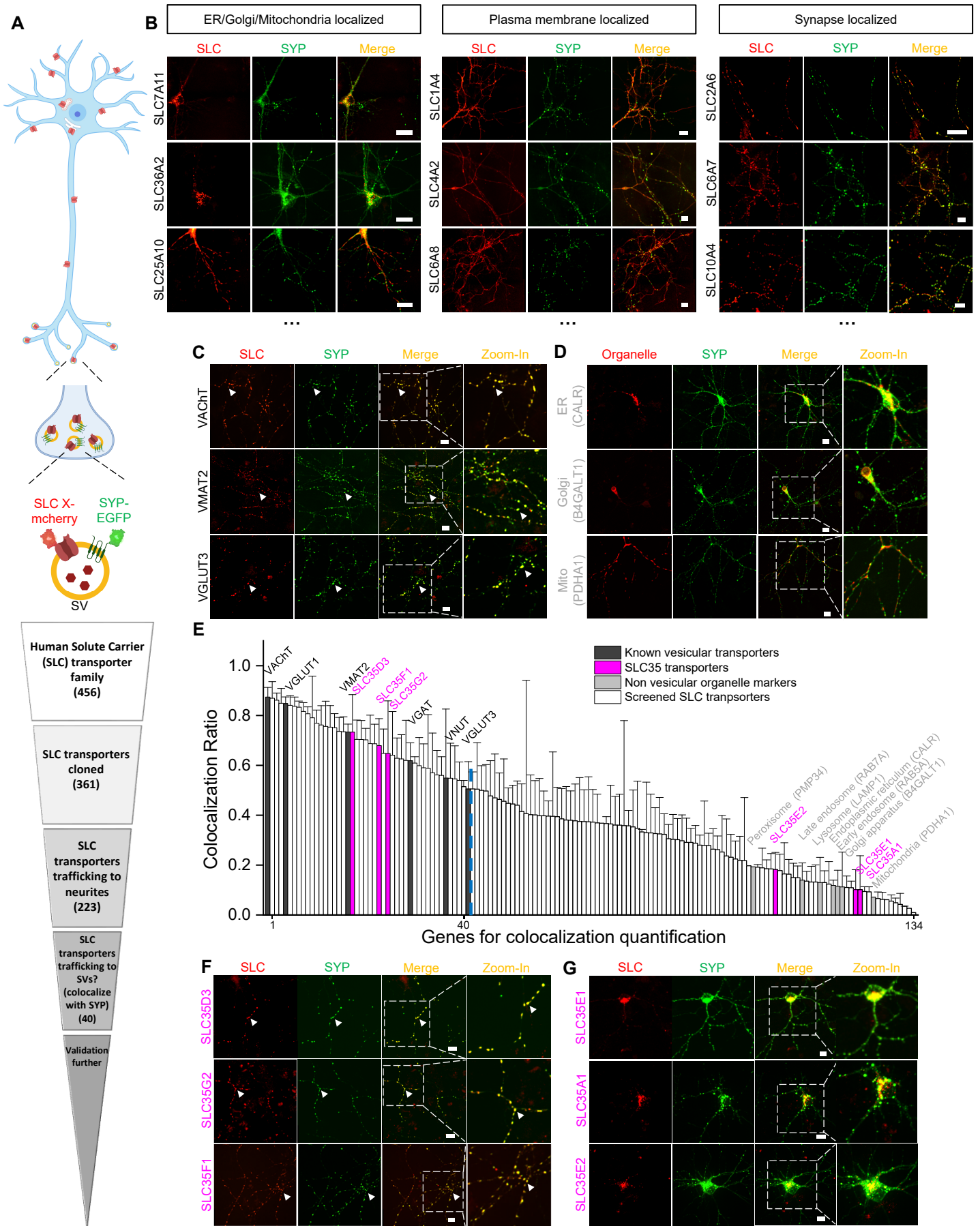
Figure 1. Localization profiling of SLC family members reveals candidate vesicular transporters
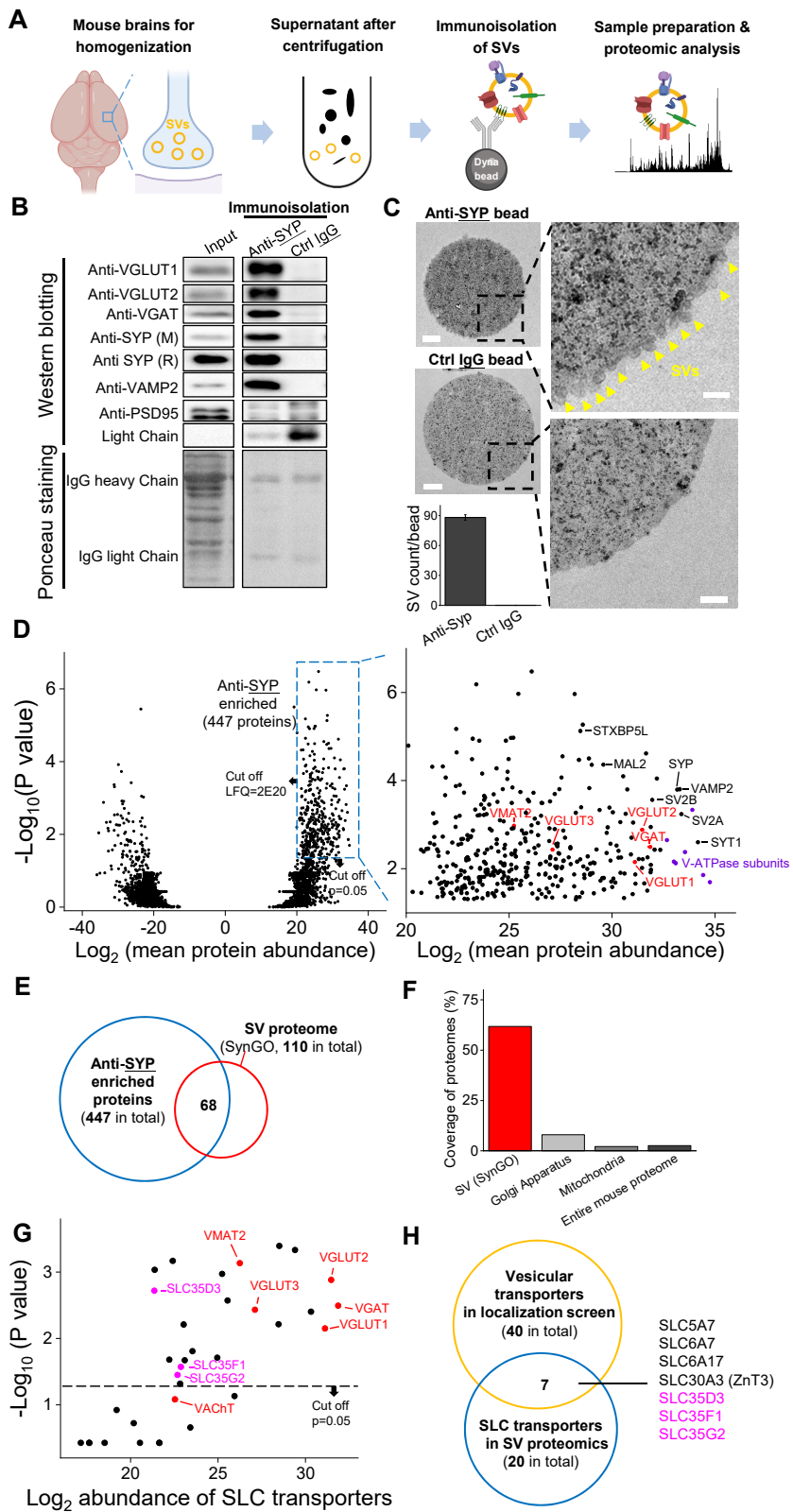
Figure 2. Proteomics profiling of SVs identifies novel putative vesicular SLC transporters
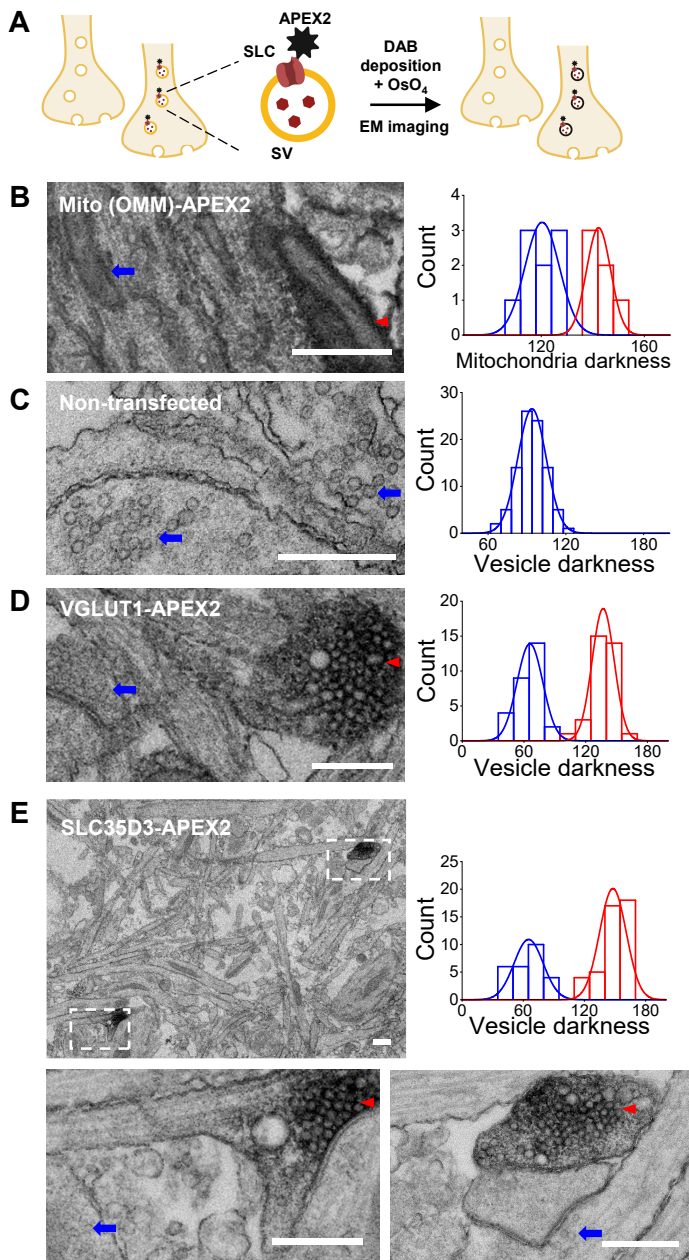
Figure 3. Validation of the vesicular localization of SLC35D3 using electron microscopy
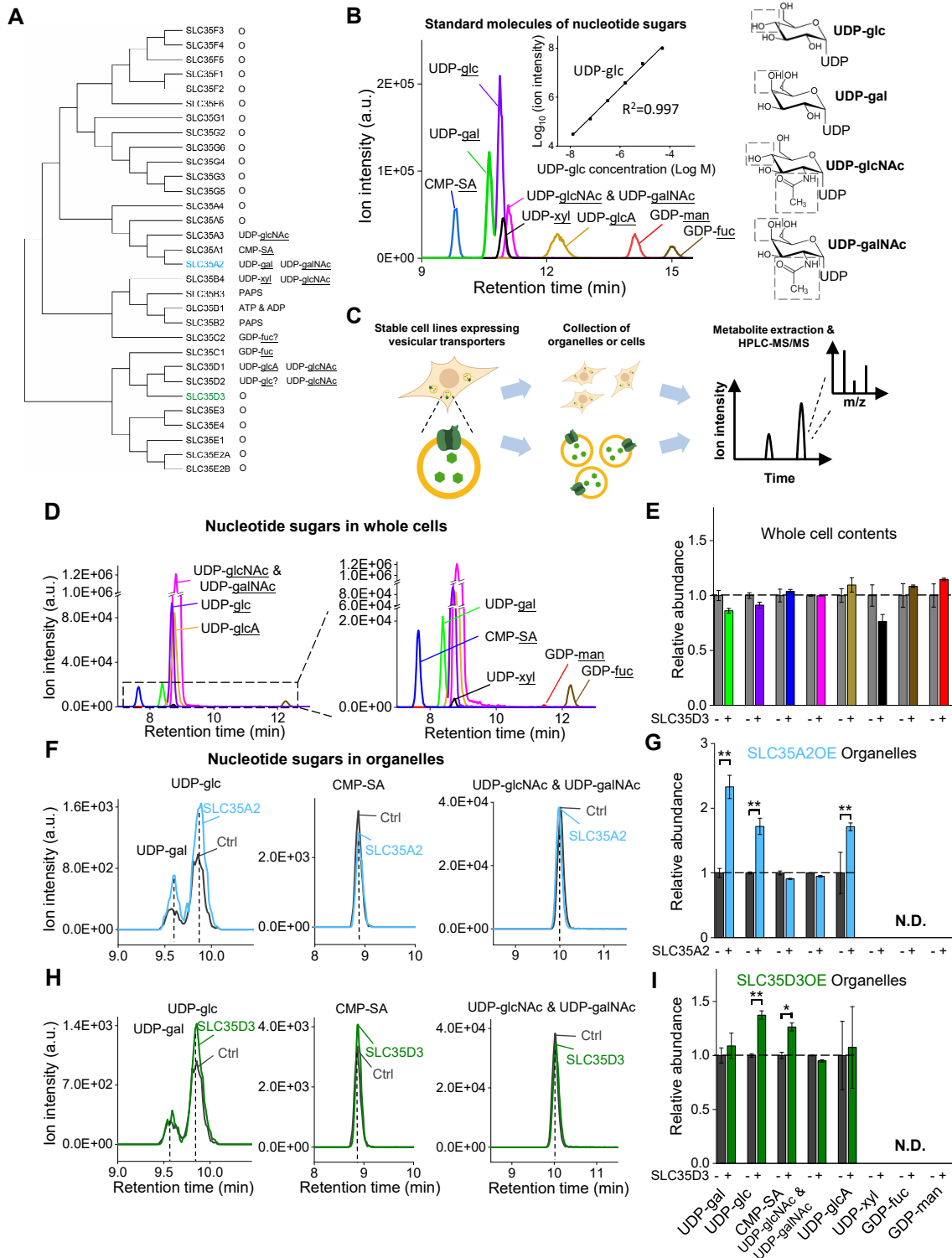
**Figure 4. The targeted metabolite profiling reveals putative substrates of SLC35D3**
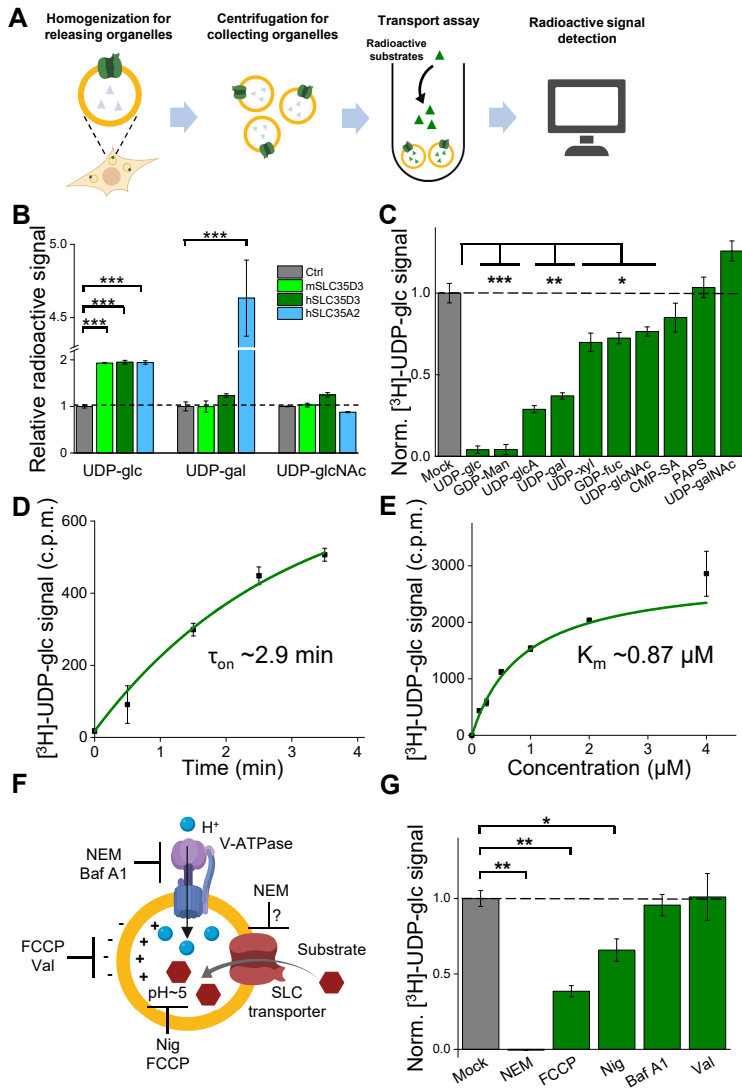
Figure 5. Validation and characterization of the UDP-glucose transport activity of SLC35D3
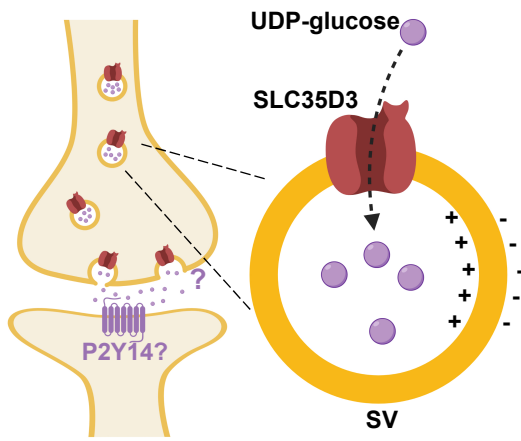
Figure 6. Working model depicting SLC35D3 as a UDP-glucose transporter on SVs

A
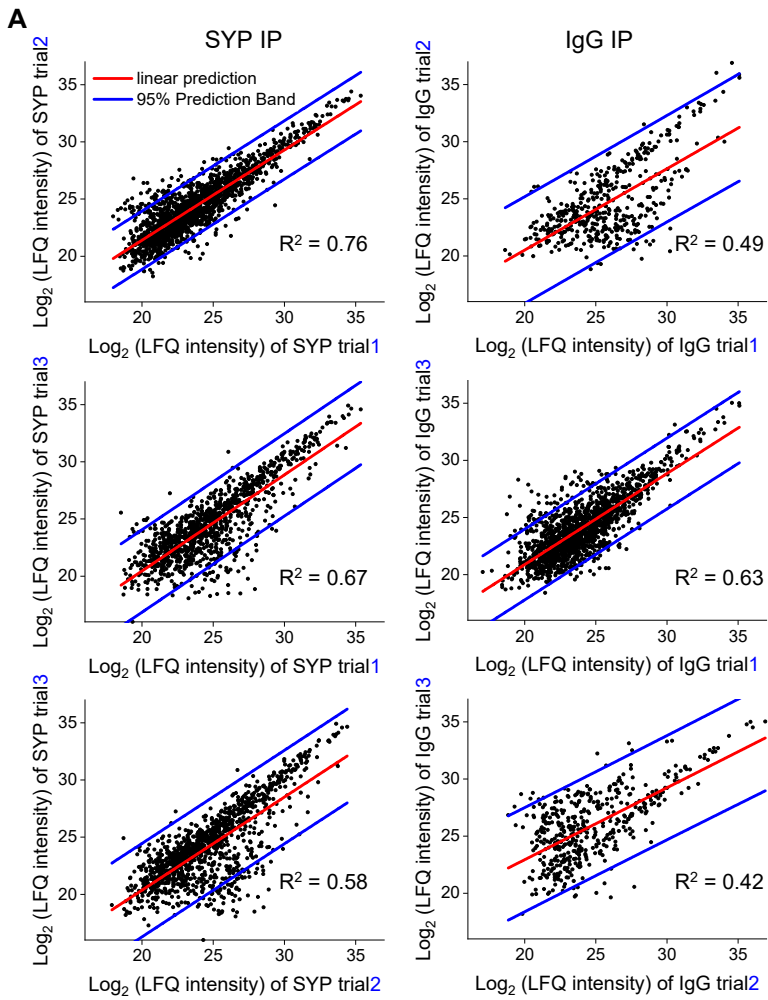
Supplementary Figure S1. Repeatability of the proteomic data (related to Figure 2)
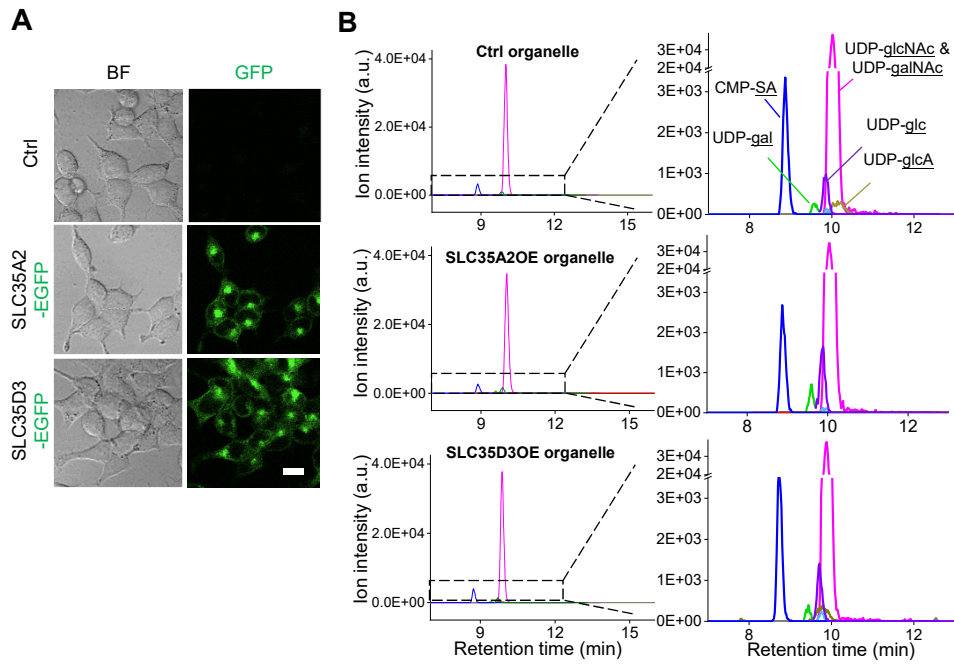
Supplementary Figure S2. Additional analysis of metabolite profiling (related to Figure 4)

Family	Transporter
Facilitative GLUT transporter family	SLC2A6
Sodium glucose cotransporter family	SLC5A3
	SLC5A7
	SLC5A12
Sodium- and chloride-dependent neurotransmitter transporter family	SLC6A7
	SLC6A14
	SLC6A17
Cationic amino acid transporter/glycoprotein-associated family	SLC7A4
Na^+/H^+ exchanger family	SLC9A1
Sodium bile salt cotransport family	SLC10A4
Folate/thiamine transporter family	SLC19A3
Organic anion transporter family	SLC21A9
Organic cation/anion/zwitterion transporter family	SLC22A6
	SLC22A24
Mitochondrial carrier family	SLC25A13
	SLC25A40
Multifunctional anion exchanger family	SLC26A11
Zinc efflux family	SLC30A3
Nucleoside-sugar transporter family	SLC35A2
	SLC35A3
	SLC35B1
	SLC35B4
	SLC35C1
	SLC35D2
	SLC35D3
	SLC35E4
	SLC35F1
	SLC35F2
	SLC35F3
	SLC35F6
	SLC35G2
Proton-coupled amino acid transporter family	SLC36A3
System A and System N sodium-coupled neutral amino acid transporter family	SLC38A4
	SLC38A6
Metal ion transporter family	SLC39A5
Basolateral iron transporter family	SLC40A1
MgtE-like magnesium transporter family	SLC41A2
Na^+-independent, system-L-like amino acid transporter family	SLC43A3
Heme transporter family	SLC48A1
Riboflavin transporter family	SLC52A3

Supplementary table 1. Vesicular transporters identified in SLC localization profiling, related to Figure 1

Family	Transporter	Reported	Ref
Vesicular glutamate transporter	SLC17A6 (VGLUT2)	Yes	Known vesicular transporters
	SLC17A7 (VGLUT1)	Yes	
	SLC17A8 (VGLUT3)	Yes	
Vesicular amine transporter	SLC18A2 (VMAT2)	Yes	
	SLC18A3 (VAChT)	Yes	
Vesicular inhibitory amino acid transporter	SLC32A1 (VGAT)	Yes	
Zinc efflux family	SLC30A3 (ZNT3)	Yes	*Proceedings of the National Academy of Sciences 93.25 (1996):* 14934-14939.
Facilitative GLUT transporter	SLC2A3	Yes	*The Journal of Neuroscience :* (2010):2-12.
	SLC2A13	Yes	*Cell* 127.4 (2006): 831-846
Cationic amino acid transporter/glycoprotein-associated	SLC7A14	Yes	*Cell* 127.4 (2006): 831-846
Na$^+$/Ca^{2+} exchanger	SLC8A1	Yes	*The Journal of Neuroscience :* (2010):2-12.
	SLC8A2	Yes	*The Journal of Neuroscience :* (2010):2-12.
Na$^+$/H$^+$ exchanger	SLC9A7	Transport activity reported	*Nature neuroscience* 14.10 (2011): 1285.
Sodium- and chloride-dependent neurotransmitter transporter	SLC6A7	Yes	*Journal of Neuroscience* 19.1 (1999): 21-33.
	SLC6A17	Yes	*Molecular pharmacology* 74.6 (2008): 1521-1532. *Journal of Biological Chemistry* 284.13 (2009): 8439-8448.
	SLC6A1	No	
Heavy subunits of the heteromeric amino acid transporter	SLC3A2	No	
Bicarbonate transporter	SLC4A10	No	
Sodium glucose cotransporter	SLC5A7	No	
Electroneutral cation-coupled Cl cotransporter	SLC12A7	No	
	SLC12A6	No	
	SLC12A9	No	
Type III Na$^+$-phosphate cotransporter	SLC20A2	No	
Organic cation/anion/zwitterion transporter	SLC22A17	No	
Nucleoside-sugar transporter	SLC35D3	No	
	SLC35F1	No	
	SLC35G2	No	

Supplementary table 2. SLC transporters enriched in immunoisolated synaptic vesicles, related to Figure 2